MHD Flow and Heat Transfer Analysis of Micropolar Fluid through a Porous Medium between Two Stretchable Disks Using Quasi-Linearization Method

Akhter, Shaheen; Ashraf, Muhammad
Centre for Advanced Studies in Pure and Applied Mathematics (CASPAM), Bahauddin Zakariya University Multan, PAKISTAN

Ali, Kashif*+
Department of Basic Sciences and Humanities, Muhammad Nawaz Shareef University of Engineering and Technology, Multan, Pakistan

ABSTRACT: *In this paper, a comprehensive numerical study is presented for studying the MHD flow and heat transfer characteristics of Non-Newtonian micropolar fluid through a porous medium between two stretchable porous disks. The system of governing equations is converted into coupled nonlinear ordinary ones through a similarity transformation, which is then solved using Quasi-linearization method. The effects of the magnetic field, the vortex viscosity, the microinertia density, the spin gradient viscosity, the stretching of the disks, the viscous dissipation, the ratio of momentum diffusivity to thermal viscosity, the radiation and the porosity of the medium on the flow, microrotation and temperature fields are discussed through tables and graphs.*

KEYWORDS: *MHD; Stretchable disks; Porous medium; Heat transfer; Quasi-linearization.*

INTRODUCTION

Flow between two disks has applications in the fields of heat exchangers, lubricants, rotating machineries, viscometries and oceanography. In thrust bearings, the disks are separated by means of a lubricant injected through the disks. Moreover, the fluids with polymer additives have been used as improved lubricants in the modern lubrication technology [1]. The imposed injection/suction through a porous surface is of general interest in many practical applications including film cooling, supercritical boilers, control of boundary layer etc. Fluid flows and thermal characteristics in rotor-stator systems play an important role in the turbo machinery and power engineering.

Darcy [2] presented the Darcy's law, which describes the mathematical modeling of the fluid flow through porous medium. The law was formulated on the basis of experimental results related to the water flow through beds of sand. Many researchers have employed the law

** To whom correspondence should be addressed.*
+ E-mail: kashifali-381@yahoo.com
1021-9986/2017/4/155-169 15/$/6.50

in their investigations. For example, *Rashidi et al.* [3] used the homotopy analysis method to describe the analytical solution for the steady flow in a porous medium over a rotating disk. Analytical series solution of nonlinear ODEs was carefully tested for convergence, and was also validated by comparing with the shooting methodology based on the 4th order RK method. *Yoon et al.* [4] numerically investigated the problem of flow and heat transfer over a steadily rotating (about longitudinal axis) infinite disk, with surface roughness. Unsteady flow over a stretchable rotating disk with deceleration was studied numerically by *Fang* [5]. Instabilities occurring in the flow between two rotating disks, enclosed by a rotating cylinder, were discussed experimentally by *Gauthier et al.* [6]. Flow between two counter rotating infinite disks was investigated by *Rentrop et al.* [7], using the shooting method. *Hamza et al.* [8] presented the exact solution for the unsteady MHD oscillatory fluid flow through a porous medium, and studied the effects of the slip condition. Numerical simulation of unsteady water-based nanofluid flow between two orthogonally moving porous disks was presented by *Ali et al.* [9].

There are a number of fluids which are important from the industrial point of view, and display non-Newtonian behavior. Due to the complexity of such fluids, several models have been proposed but the micropolar model is the most prominent one. *Hoyt and Fabula* [10] experimentally showed that the fluids, which could not be characterized by the classical Newtonian relationships, indicated significant reduction in the shear stress near a rigid body, and could be well explained by the micropolar model introduced by *Eringen* [11-12]. The micropolar fluid is an active area of research, and therefore many researchers have investigated the related flow and heat transfer problems. For example, *Ashraf and Wehagal* [13] discussed the numerical solution for electrically conducting micropolar fluid flow between two infinite parallel porous disks. *Hayat et al.* [14] presented the problem of MHD axisymmetric flow of 3rd grade fluid between two porous disks, and used the homotopy analysis method for solving the nonlinear ODEs obtained by applying the similarity transformation to the governing set of PDEs. *Ramachadraoo* [15] provided the exact solution for the unsteady micropolar fluid flow due to essentially rotating disks. Flow and heat transfer analysis of steady axisymmetric incompressible MHD micropolar fluid between two infinite disks was presented by *Ashraf et al.* [16]. The governing nonlinear equations were converted into coupled nonlinear ODEs with the help of Von-Karman transformation, whereas the solution was obtained numerically with the help of a finite difference scheme. *Muthu et al.* [17] presented the problem of oscillatory micropolar fluid flow in an annular region, and employed the perturbation method to solve the governing nonlinear equations. The revolving ferrofluid flow over rotating disk was considered by *Paras* [18], using the Neuringer-Rosensweig model. *Turkyilmazoglu* [19] investigated the fluid flow and heat transfer occurring between two stretchable disks rotating co-axially at constant distance apart. It was noted that the stretching action of a disk surface altered considerably the classical flow behavior occurring between two disks. The recent investigations on the fractal models and fractal-based approaches that are applied for effective thermal conductivity, convective heat transfer, critical heat flux and sub-cooled pool boiling of nanofluids, fractal clusters and yield stress property of nanoparticle aggregation are summarized in the excellent review by *Cai et al.* [20]. A comprehensive literature review on the micropolar fluid flow in different geometries under various conditions may be found in *Ashraf et al.* [21-24].

We suggest the *Ariman et al.* [25]-[26], *Eringen* [27], and *Lukaszewicz* [28] as excellent resources for the literature on micropolar fluids. Moreover, for the review of scientific literature related to the effect of stretching/shrinking surfaces on the flow and thermal characteristics of different problems, we recommend *Abolbashari et al.* [29], *Rashidi et al.* [30-32], *Aghajani et al.* [33], *Ali et al.* [34], *Akram et al.* [35], *Khan et al.* [36] and *Nadeem et al.* [37] as very good references.

In the present work, we explore the flow and thermal characteristics of a viscous, incompressible and electrically conducting micropolar fluid through the porous medium between two stretchable infinite disks, under the action of a uniform transverse magnetic field. An appropriate similarity transformation has been employed for obtaining the governing nonlinear ODEs, which are then solved numerically. We have noted that the micropolar structure of the fluid reduces both the shear stress and the heat transfer at the disks, whereas the stretching of the disks exhibits an opposite trend. Further, the porous medium has the tendency of increasing

the shear as well as the couple stresses, and the heat transfer rate at both the disks.

MATHEMATICAL MODEL

We consider the steady, viscous, laminar and incompressible flow of an electrically conducting micropolar fluid through a porous medium between two stretchable infinite disks, situated at z=-h and z=h as shown in the Fig. 1. Further, a uniform transverse magnetic field is assumed to be acting normally on the flow, whereas the two disks are being stretched at the same rate. The cylindrical polar coordinate system is noted to be most appropriate for the present study. The induced magnetic field can be neglected as compared to the imposed magnetic field as the magnetic Reynolds number is assumed to be small (*Shercliff* [38]). The electric field is zero as we have supposed that there is no polarization voltage is applied. The components of microrotation $(\upsilon_1,\upsilon_2,\upsilon_3)$ and velocity (*u,v,w)* along the transverse, radial and axial directions can be written as

$$\upsilon_1=0,\ \upsilon_2(r,z),\ \upsilon_3=0,\ u_z=u_z(r,z),\qquad u_r=u_r(r,z),\ u_\theta=0 \tag{1}$$

By analyzing Eq. (1), and following *Ashraf et al.* [21-24], the governing equations of the problem under consideration can be given as:

$$\frac{u_r}{r}+\frac{\partial u_r}{\partial r}+\frac{1}{h}\frac{\partial u_z}{\partial \eta}=0 \tag{2}$$

$$\rho\left(u_r\frac{\partial u_r}{\partial r}+\frac{u_z}{h}\frac{\partial u_r}{\partial \eta}\right)=-\frac{\partial p}{\partial r}-\frac{\kappa}{h}\frac{\partial \upsilon_2}{\partial \eta}+(\mu+\kappa)\left(\frac{\partial^2 u_r}{\partial r^2}+\frac{1}{r}\frac{\partial u_r}{\partial r}-\frac{u_r}{r^2}+\frac{1}{h^2}\frac{\partial^2 u_r}{\partial \eta^2}\right)-\sigma_e B_\circ^2 u_r-\frac{(\mu+\kappa)}{\kappa^\bullet}u_r \tag{3}$$

$$\rho\left(u_r\frac{\partial u_z}{\partial r}+\frac{u_z}{h}\frac{\partial u_z}{\partial \eta}\right)=-\frac{1}{h}\frac{\partial p}{\partial \eta}+\kappa\left(\frac{\partial \upsilon_2}{\partial r}+\frac{\upsilon_2}{r}\right)+(\mu+\kappa)\left(\frac{\partial^2 u_z}{\partial r^2}+\frac{1}{r}\frac{\partial u_z}{\partial r}+\frac{1}{h^2}\frac{\partial^2 u_z}{\partial \eta^2}\right)-\frac{(\mu+\kappa)}{\kappa^\bullet}u_z \tag{4}$$

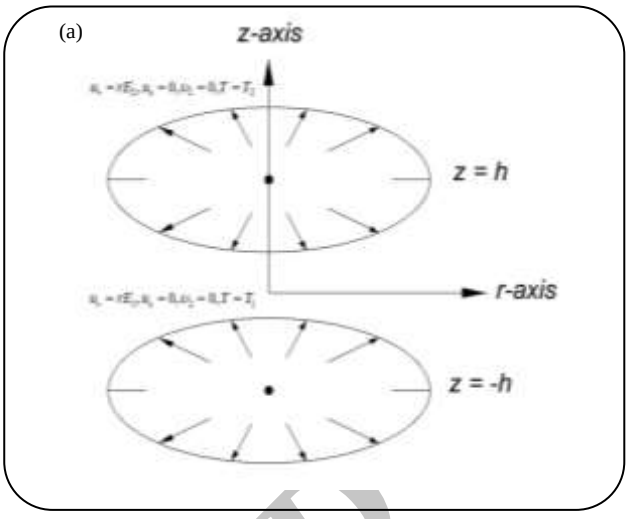

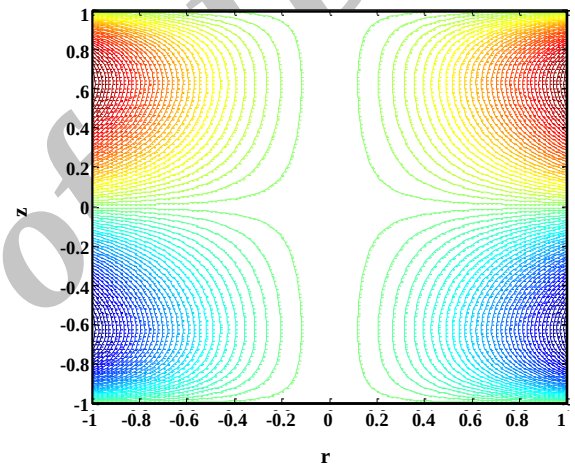

Fig. 1: a) Physical Configuration of the problem. b) Streamlines for the flow for M=1, α =1, C1=1, C2=0.2, C3=0.3, Ec=1, ε =1, Nr=1, Pr=1.

$$d\rho j\left(u_r\frac{\partial \upsilon_2}{\partial r}+\frac{u_z}{h}\frac{\partial \upsilon_2}{\partial \eta}\right)=\kappa\left(\frac{1}{h}\frac{\partial u_r}{\partial \eta}-\frac{\partial u_z}{\partial r}\right)-d2\kappa\upsilon_2+\gamma\left(\frac{\partial^2 \upsilon_2}{\partial r^2}-\frac{\upsilon_2}{r^2}+\frac{1}{r}\frac{\partial \upsilon_2}{\partial r}+\frac{1}{h^2}\frac{\partial^2 \upsilon_2}{\partial \eta^2}\right) \tag{5}$$

Here, ρ is the density, η is the dimensionless coordinate in the axial direction, $k^\bullet$ is the Darcy permeability, *j* is the microinertia, *p* is the pressure, μ is the dynamic viscosity of the fluid, κ is the vortex viscosity, γ is the spin gradient viscosity, B_o is the strength of magnetic field, and σ_e is the electrical conductivity. Considering the thermal radiation and

viscous dissipation effects, the energy equation takes the form:

$$\rho c_p\left(u_r\frac{\partial T}{\partial r}+\frac{u_z}{h}\frac{\partial T}{\partial \eta}\right)=k_\circ\left(\frac{1}{h^2}\frac{\partial^2 T}{\partial \eta^2}+\frac{\partial^2 T}{\partial r^2}+\frac{1}{r}\frac{\partial T}{\partial r}\right)- \quad (6)$$
$$\frac{\partial q_r}{\partial r}+\frac{\mu}{h^2}\left(\frac{\partial u_r}{\partial \eta}\right)^2$$

Where c_p is the specific heat capacity, T is the temperature, q_r is the radiative heat flux and k_o is the thermal conductivity of the fluid.

In view of the Rosseland approximation for radiation (please see *Devi and Devi* [39]), the radiative heat flux q_r may be written as

$$q_r=-\frac{4\sigma}{3k^*}\frac{\partial T^4}{\partial z} \quad (7)$$

Where σ and k^* are the Stefan-Boltzmann constant and the mean absorption coefficient, respectively. Now, the term T^4 in the above expression is linearized by expanding it in a Taylor series about T_∞, to get:

$$T^4\cong 4T_\infty^3T-3T_\infty^4 \quad (8)$$

Therefore, Eq. (6) becomes:

$$\rho c_p\left(u_r\frac{\partial T}{\partial r}+\frac{u_z}{h}\frac{\partial T}{\partial \eta}\right)-k_\circ\left(\frac{1}{h^2}\frac{\partial^2 T}{\partial \eta^2}+\frac{\partial^2 T}{\partial r^2}+\frac{1}{r}\frac{\partial T}{\partial r}\right)- \quad (9)$$
$$\frac{16\sigma T_\infty^3}{3k^*}\frac{\partial^2 T}{\partial z^2}-\frac{\mu}{h^2}\left(\frac{\partial u_r}{\partial \eta}\right)^2=0$$

The boundary conditions for the problem may be given as,

$$\left.\begin{array}{l} u_r(r,-h)=rE_1, u_r(r,h)=rE_2,\\ u_z(r,-h)=0, u_z(r,h)=0,\\ \upsilon_2(r,-h)=0,\ \upsilon_2(r,h)=0,\\ T(r,-h)=T_1, T(r,h)=T_2 \end{array}\right], \quad (10)$$

Where E_1 and E_2 are the stretching strengths of the lower and upper disks (respectively),both having units of *1/t* The system of partial differential Eqs. (3) - (5) and (9) may be transformed into ordinary ones,by using the following similarity transformation:

$$\eta=\frac{z}{h},\ u_r=-\frac{rE_1}{2}f'(\eta),\ \upsilon_2=-\frac{rE_1}{2h}g(\eta), \quad (11)$$
$$u_z=E_1hf(\eta),\ \theta(\eta)=\frac{T-T_2}{T_1-T_2},$$

Where T_1 and T_2 are the fixed temperatures of the lower and the upper disks respectively. We note that the continuity equation is identically satisfied by the velocity field given in Eq. (11), and hencerepresents a possible fluid motion.

Now, the system of governing equations, in view of Eq. (11), reduces to:

$$(1+C_1)f'''-Rff''-C_1g''-\left(M^2R+(1+C_1)\varepsilon\right)f''=0 \quad (12)$$

$$C_3g''+C_1(f''-2g)+RC_2\left(\frac{f'g}{2}-fg'\right)=0 \quad (13)$$

$$\left(1+\frac{4}{3}Nr\right)\theta''-RPrf\theta'+\frac{1}{4}PrEcf''^2=0 \quad (14)$$

Here, $M=\sqrt{\frac{\sigma_e B_\circ^{\ 2}}{\rho E_1}}$ is the magnetic parameter, $C_1=\kappa/\mu$ is the vortex viscosity parameter, $C_2=j/h^2$ is the microinertia density parameter, $C_3=\gamma/\mu h^2$ is the spin gradient viscosity parameter, $R=\rho E_1h^2/\mu$ is the stretching Reynolds number, $Ec=r^2E_1^{\ 2}/c_p(T_1-T_2)$ is the Eckert number, $Pr=\mu c_p/k_\circ$ is the Prandtl number, $Nr=4\sigma T_\infty^3/k^*k_\circ$ is the radiation parameter and $\varepsilon=h^2/k^\bullet$ is the porosity parameter. The boundary conditions (10) get the form:

$$f(-1)=f(1)=0,\ f'(-1)=-2,\ f'(1)=-2\alpha, \quad (15)$$
$$g(-1)=0,\ g(1)=0,\ \theta(-1)=1,\ \theta(1)=0,$$

Where $\alpha=E_2/E_1$ is the relative disk stretching parameter.

It is worth mentioning that, for the classical Newtonian fluid, Eqs. (12)-(15) reduce to the ones given by *Turkyilmazoglu* [19].

COMPUTATIONAL PROCEDURE

For the numerical solution, we employ Quasi-linearization as follows:

The sequences of vectors $d\left\{f^{(k)}\right\}$, $\left\{g^{(k)}\right\}$ and $\left\{\theta^{(k)}\right\}$ are constructed, which converge to the numerical solution of Eqs. (12)-(13) and Eq. (14) respectively. To construct $\left\{f^{(k)}\right\}$, we linearize Eq. (12) by retaining only the first order terms. For this, we first set:

$$G\left(f,f',f'',f''',f''''\right)=$$
$$\left(1+C_1\right)f''''-Rff'''-C_1g''-\left(M^2R+\left(1+C_1\right)\varepsilon\right)f''$$

which leads to:

$$G\left(f^{(k)},f'^{(k)},f''^{(k)},f'''^{(k)},f''''^{(k)}\right)+\left(f^{(k+1)}-f^{(k)}\right)\frac{\partial G}{\partial f^{(k)}}+$$
$$\left(f'^{(k+1)}-f'^{(k)}\right)\frac{\partial G}{\partial f'^{(k)}}+\left(f''^{(k+1)}-f''^{(k)}\right)\frac{\partial G}{\partial f''^{(k)}}+$$
$$\left(f'''^{(k+1)}-f'''^{(k)}\right)\frac{\partial G}{\partial f'''^{(k)}}+\left(f''''^{(k+1)}-f''''^{(k)}\right)\frac{\partial G}{\partial f''''^{(k)}}=0$$

After simplification, one arrives at:

$$\left(1+C_1\right)f^{iv(k+1)}-Rf^{(k)}f'''^{(k+1)}-\left\{RM^2+\left(1+C_1\right)\varepsilon\right\}f''^{(k+1)}-$$
$$Rf^{(k+1)}f^{(k)}=C_1g''-f^{(k)}f'''R$$

which turns into:

$$\left\{\left(1+C_1\right)+0.5\Delta\eta Rf_i^{(k)}\right\}f_{i-2}^{(k+1)}+ \qquad (16)$$
$$\left\{-4\left(1+C_1\right)-\Delta\eta Rf_i^{(k)}-\Delta\eta^2R\left(M^2+\left(1+C_1\right)\varepsilon\right)\right\}f_{i-1}^{(k+1)}+$$
$$\left\{6\left(1+C_1\right)+2\Delta\eta^2R\left(M^2+\left(1+C_1\right)\varepsilon\right)-\right.$$
$$\left.0.5\Delta\eta R\left(-f_{i-2}^{(k)}+2f_{i-1}^{(k)}-2f_{i+1}^{(k)}+f_{i+2}^{(k)}\right)\right\}f_i^{(k+1)}+$$
$$\left\{-4\left(1+C_1\right)+\Delta\eta Rf_i^{(k)}-\Delta\eta^2R\left(M^2+\left(1+C_1\right)\varepsilon\right)\right\}f_{i+1}^{(k+1)}+$$
$$\left\{\left(1+C_1\right)-0.5\Delta\eta Rf_i^{(k)}\right\}f_{i+2}^{(k+1)}=$$
$$\Delta\eta^2\left(g_{i-1}^{(k)}-2g_i^{(k)}+g_{i+1}^{(k)}\right)C_1-$$
$$0.5\Delta\eta R\left(-f_{i-2}^{(k)}+2f_{i-1}^{(k)}-2f_{i+1}^{(k)}+f_{i+2}^{(k)}\right)f_i^{(k)}$$

on the subject. The parameters of the study are the Reynolds number R, the magnetic parameter M, the Eckert number E_C the micropolar parameters C_1, C_2, C_3 the radiation parameter Nr, the Prandtl number Pr, and the porosity parameter ε. Physical quantities of our concern are the shear stress, the couple stress and the heat transfer rate at the disks. The shear stress τ_w, the wall couple stress C_g and the nusstle number *Nu* at the two disks, are given by:

$$\tau_w=\left(\mu+\kappa\right)\left(\frac{\partial u}{\partial z}+\frac{\partial w}{\partial r}\right)_{z=\pm h}=\left(1+C_1\right)f''\left(\pm1\right),$$

$$C_g=\frac{\gamma\left(\frac{\partial\upsilon_2}{\partial z}\right)_{z=\pm h}}{\rho\left(rE\right)^2}=\frac{1}{2}\frac{C_3}{Re_r}g'\left(\pm1\right),$$

$$Nu=\frac{hq_w}{k\left(T_1-T_2\right)}=\frac{-h\left(\frac{\partial T}{\partial z}\right)_{z=\pm h}}{k\left(T_1-T_2\right)}=-\theta'\left(\pm1\right),$$

Where $Re_r=\rho Ehr/\mu$ is the local Reynolds number.

It is obvious that the shear stress, the couple stress and the heat transfer rate are proportional to the values of $f''(\eta),g'(\eta)\text{and}\theta'(\eta)$, respectively, at the two disks. That is why, in order to study the effect of the governing parameters on the above mentioned physical quantities, we shall see (in the Tables 1-9) how the values of $f''\left(\pm1\right)$, $g'\left(\pm1\right)$ and $\theta'\left(\pm1\right)$ are affected by these parameters.

Table 1 shows the convergence of our numerical results as the step-size decreases, which makes us confident about our computational procedure. Table 2 predicts that the viscous dissipation enhances the heat transfer rate at the lower as well as the upper disk. Tables 3 and 4 show that the stretching Reynolds number and the applied magnetic field may increase the shear andthe couple stresses at both the disks. Further, the Reynolds number has the tendency of increasing the heat transfer rate. On the other hand, the heat transfer rate at the upper disk first decreases and then increases by increasing the strength of the external magnetic field. Table 5 represents the effect of the porosity parameter ε on the physical quantities which we are interested in. It is obvious that the porosity of the medium is responsible for enhancing the magnitude of the shear and the couple stresses, as well as the heat transfer rate at the disks. Influence of the disk stretching parameter α on the shear & couple

Table 1: Dimensionless temperature $\theta(\eta)$ on three grid sizes and extrapolated values for $R = 5, M = 0.5, C_1 = 1.4, C_2 = 0.7, C_3 = 1, Pr = 1.7, Ec = 1.6, Nr = 0.2$.

$\theta(\eta)$				
η	1st grid (h = 0.02)	2nd grid (h = 0.01)	3rd grid (h = 0.005)	Extrapolated Values
-0.8	1.940438	1.941475	1.941734	1.941821
-0.4	2.171709	2.173308	2.173708	2.173841
0	2.078009	2.079664	2.080078	2.080216
0.4	1.954176	1.955803	1.956210	1.956346
0.8	1.295799	1.296841	1.297102	1.297188

Table 2: The effect of viscous dissipation on heat transfer rate with $R = 5, \alpha = 1, C_1 = 1.4, C_2 = 0.7, C_3 = 1, Pr = 1.7, M = 0.5, \varepsilon = 1, Nr = 0.2$.

Ec	θ' (-1)	θ' (1)
0.0	-0.955429	-0.955429
0.1	-0.415180	-1.495678
0.2	0.125069	-2.035928
0.3	0.665318	-2.576176
0.4	1.205567	-3.116426

Table 3: The effect of stretching Reynolds number on shear & couple stresses and heat transfer rate with $M = 0.5, \alpha = 1, C_1 = 1.4, C_2 = 0.7, C_3 = 1, Ec = 1.6, \varepsilon = 1, Nr = 0.3, Pr = 1.7$.

R	f'' (-1)	g' (-1)	θ' (-1)	f'' (1)	g' (1)	θ' (1)
0	5.670487	2.376847	5.327080	-5.670487	2.376847	-6.327080
5	8.939008	2.484744	6.642213	-8.939008	2.484744	-8.391086
10	11.207192	2.522483	7.661974	-11.207192	2.522483	-10.040432
15	12.975845	2.536483	8.512650	-12.975845	2.536483	-11.445432
20	14.444564	2.539721	9.246482	-14.444564	2.539721	-12.680963

Table 4: The effect of magnetic parameter on shear & couple stresses and heat transfer rate with $R = 5, \alpha = 1, C_1 = 1.4, C_2 = 0.7, C_3 = 1, Ec = 1.6, \varepsilon = 1, Nr = 0.2, Pr = 1.7$.

M	f'' (-1)	g' (-1)	θ' (-1)	f'' (1)	g' (1)	θ' (1)
0.6	8.114244	2.471847	7.687023	-8.114244	2.471847	-9.590865
1.2	8.733742	2.482903	7.593713	-8.733742	2.482903	-9.456728
1.8	9.658834	2.498659	7.625419	-9.658834	2.498659	-9.431269
2.4	10.788859	2.516574	7.858604	-10.788859	2.516574	-9.600829
3.0	12.045345	2.534704	8.278842	-12.045345	2.534704	-9.958017

Table 5: The effect of porosity parameter on shear & couple stresses and heat transfer rate with $R = 5$, $\alpha = 1$, $C_1 = 1.4$, $C_2 = 0.7$, $C_3 = 1$, $Ec = 1.6$, $M = 1.5$, $Nr = 0.2$, $Pr = 1.7$.

ε	f'' (-1)	g' (-1)	θ' (-1)	f'' (1)	g' (1)	θ' (1)
1	8.939008	2.484744	7.554453	-8.939008	2.484744	-9.392476
2	9.999659	2.501375	7.685416	-9.999659	2.501375	-9.455637
3	10.916128	2.514404	7.939991	-10.916128	2.514404	-9.656714
4	11.728538	2.524864	8.239419	-11.728538	2.524865	-9.912532
5	12.461779	2.533415	8.552013	-12.461779	2.533415	-10.188686

Table 6: The effect of disk stretching parameter on shear & couple stresses and heat transfer rate with $R = 4$, $Ec = 1.6$, $C_1 = 1.4$, $C_2 = 0.7$, $C_3 = 1$, $Pr = 1.7$, $M = 0.5$, $\varepsilon = 1$, $Nr = 0.3$.

α	f'' (-1)	g' (-1)	θ' (-1)	f'' (1)	g' (1)	θ' (1)
0.0	6.178077	2.125453	2.184717	-1.299126	0.325465	-0.479008
0.2	6.483157	2.185999	2.886097	-2.446969	0.748515	-1.122362
0.4	6.765655	2.249195	3.697053	-3.640437	1.174699	-2.182835
0.6	7.027430	2.315095	4.589566	-4.879718	1.602266	-3.696987
0.8	7.270225	2.383699	5.525349	-6.164835	2.029539	-5.679009
1.0	7.495665	2.454954	6.460911	-7.495665	2.454954	-8.117442

Table 7(a): Four cases of values of micropolar parameters C_1, C_2 & C_3.

Case No.	C_1	C_2	C_3
1(Newtonian)	0.0	0.0	0.0
2	0.5	0.1	0.4
3	1.0	0.2	0.8
4	1.5	0.3	1.6

Table7(b): The effect of micropolar parameters C_1, C_2 & C_3 on shear & couple stresses and heat transfer rate with $R = 5$, $M = 5$, $\alpha = 1$, $Ec = 1.6$, $\varepsilon = 1$, $Nr = 0.2$, $Pr = 1.7$.

Cases	f'' (-1)	g' (-1)	θ' (-1)	f'' (1)	g' (1)	θ' (1)
1	23.292101	0	14.238388	-23.292101	0	-15.594982
2	19.864824	2.343794	12.247839	-19.864825	2.343794	-13.670562
3	17.790088	2.331542	11.085833	-17.790088	2.331542	-12.559221
4	16.368012	2.321369	10.317662	-16.368012	2.321369	-11.831856

stresses and the heat transfer rate is shown in Table 6. Compared with the values at the lower disk, the three physical quantities are more sensitive at the upper one, with respect to the stretching parameter. Further, the parameter is noted to remarkably increase the magnitudes of all the physical quantities, at the either disk.

The cases of the values of the micropolar parameters are given in the Table 7a, whereas the Table 7b compares the values of the shear stress, the couple stress and the heat transfer rate for Newtonian fluid with those for the three cases of micropolar fluids. It is obvious that the micropolar structure of the fluid has the ability to lower

Table 8: The effect of radiation parameter on heat transfer rate with $R = 5$, $\alpha = 1$, $C_1 = 1$, $C_2 = 0.2$, $C_3 = 0.3$, $Ec = 1.6$, $M = 0.5$, $\varepsilon = 1$, $Pr = 1.7$.

Nr	θ'(-1)	θ'(1)
0.0	10.769398	-12.951851
0.2	7.672737	-9.580178
0.4	5.9172757	-7.650179
0.6	4.785562	-6.398825
0.8	3.994644	-5.521168

Table 9: The effect of Prandtl number on heat transfer rate with $R = 5$, $\alpha = 1$, $C_1 = 1.4$, $C_2 = 0.7$, $C_3 = 1$, $M = 0.5$, $\varepsilon = 1$, $Nr = 0.2$.

Pr	Ec = 0		Ec = 1.6	
	θ'(-1)	θ'(1)	θ'(-1)	θ'(1)
0.1	-0.522782	-0.522782	-0.121626	-0.923938
0.4	-0.594645	-0.594645	1.073038	-2.262328
0.7	-0.671440	-0.671440	2.369222	-3.712102
1.0	-0.752626	-0.752626	3.785278	-5.290531
1.3	-0.837565	-0.837565	5.343334	-7.018464

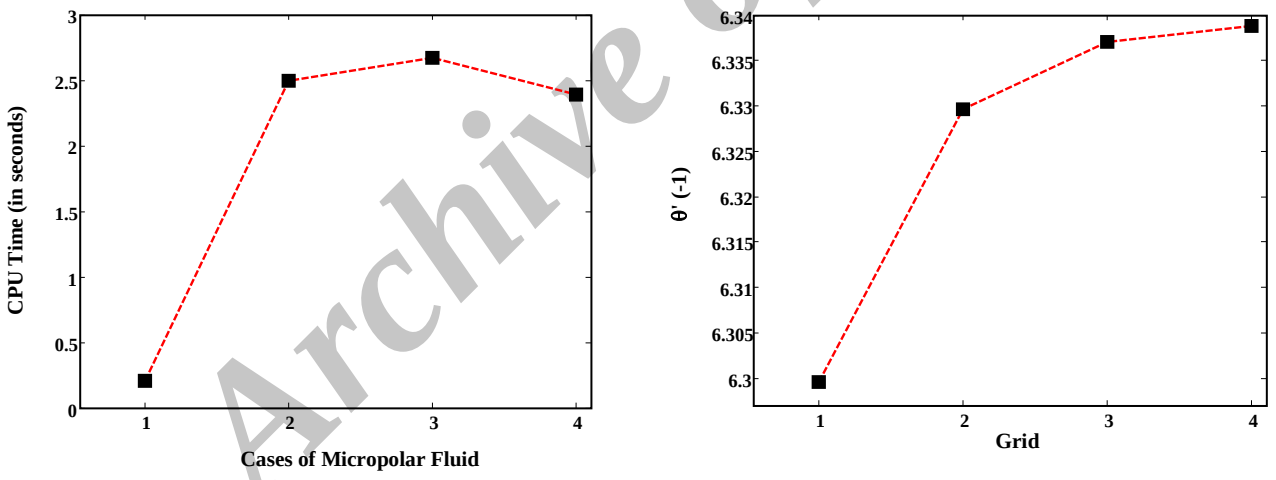

Fig. 2: a) CPU time for the four cases of the micropolar fluid, with $R = 5$, $M = 5$, $\alpha = 1$, $Ec = 1.6$, $\varepsilon = 1$, $Nr = 0.2$, $Pr = 1.7$. b) Value of $\theta'(-1)$ on the four grid sizes, with the fixed $R = 5$, $M = 5$, $\alpha = 1$, $Ec = 1.6$, $\varepsilon = 1$, $Nr = 0.2$, $Pr = 1.7$.

the wall shear stress, the couple stress and the heat transfer rate at the disks. Further, it may be noted that there is no couple stress in case of Newtonian fluid. The heat transfer rate at the lower as well as the upper disk decreases with the thermal radiation, as shown in Table 8, whereas the Table 9 shows that the heat transfer rate increases with the Prandtl number.

Now we give the interpretation of our graphical results. Physical model and the streamlines for the present problem are shown in the Figs. 1a and 1b, respectively. Fig. 2a shows the CPU time to solve the governing equations for the four cases of the micropolar parameters. It is clear that the maximum CPU time to solve the problem is well below 3 seconds, which shows

the efficiency of our numerical algorithm. Grid-independence of the values of θ'(-1) may be seen in the Fig. 2b, in which the four grids correspond to the grids with 51, 101, 201 and 401 points, respectively. Fig. 3 represents the effect of the stretching Reynolds number *R* on the axial velocity. By increasing *R*, the axial velocity decreases whereas the maximum value of the radial velocity also decreases, as shown in the Fig. 4. Moreover, the stretching of the disks has the effect of significantly decreasing the microrotation as predicted in the Fig. 5. Fig. 6 represents the variation of temperature for various *R*. It is observed that, near the lower disk, the influence of the stretching is not pronounced. However, from η= -0.8 to 0.6, the temperature profiles fall significantly. After this, the profiles rise till the upper disk.

The radiation parameterlowers the temperature profiles across the domain, whereas the viscous dissipation (characterized by the Eckert number) raises the temperature distribution to such an extent that the thermal reversal may occur near the lower disk (please see Figs. 7 and 8). It is clear from the Figs. 9-12 that the applied magnetic field has the damping effect on the velocity, microrotation and temperature fields, as all the profiles are lowered across most of the domain. Fig.13 predicts the influence of porosity parameter ε on axial velocity. The axial velocity profiles are lowered by increasing ε. The radial velocity profiles are stretched towards the boundaries and fall in the central region between the disks, with the increase of porosity as shown in Fig. 14. The microrotation profiles fall in the region near the lower disk and rise near the upper one, by increasing ε as shown in Fig. 15. The temperature profiles fall as the porosity increases as shown in Fig. 16.

Increase in the Prandtl number causes the increase in temperature acrossthe whole domain, as seen in Fig. 17. Effect of the disk stretching parameter α on the velocity, microrotation and thermal distributions may be seen from the Figs. 18-21. We notice a remarkable increase in the radial velocity and the microrotation distribution near the upper disk, whereas the thermal profiles are raised everywhere between the two disks. Finally, it is clear from the Figs. 22-25 that the micropolar structure of the fluid enhances the axial velocity, maximum value of the radial velocity, the microrotaion, and the thermal distribution across the domain.

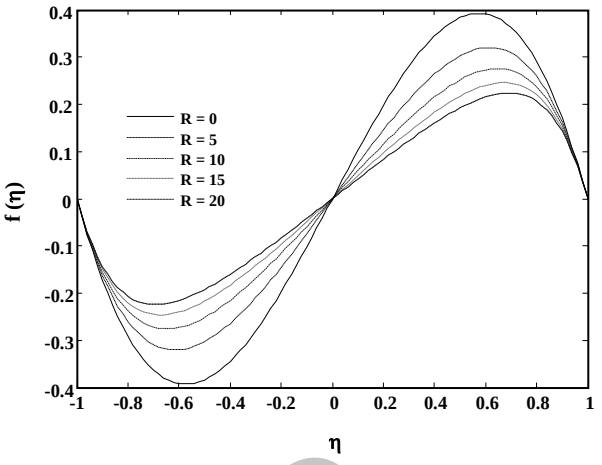

Fig. 3: Variation of axial velocity for M = 0.5, α = 1, C_1 = 1.4, C_2 = 0.7, C_3 = 1, Ec = 1.6, ε = 1, Nr = 0.3, Pr = 1.7 and various R.

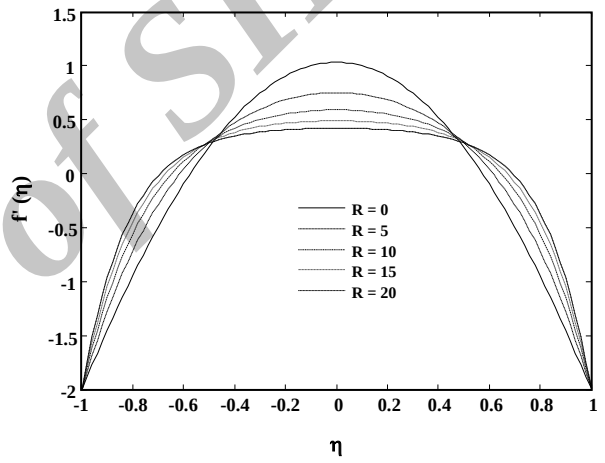

Fig. 4: Variation of radial velocity for M = 0.5, α = 1, C_1 = 1.4, C_2 = 0.7, C_3 = 1, Ec = 1.6, ε = 1, Nr = 0.3, Pr = 1.7 and various R.

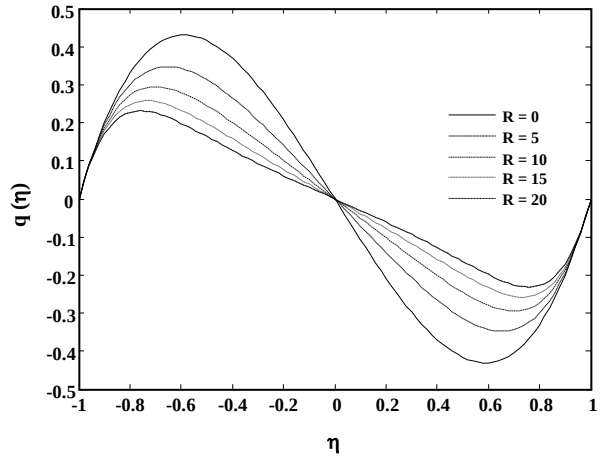

Fig. 5: Variation of microrotation for M = 0.5, α = 1, C_1 = 1.4, C_2 = 0.7, C_3 = 1, Ec = 1.6, ε = 1, Nr = 0.3, Pr = 1.7 and various R.

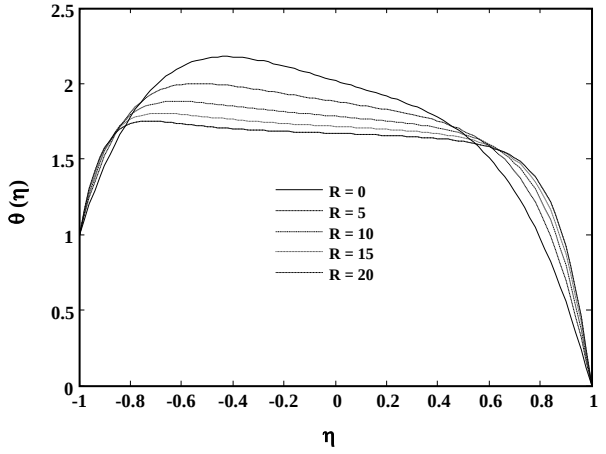

Fig. 6: Variation of temperature for M = 0.5, α = 1, C_1 = 1.4, C_2 = 0.7, C_3 = 1, Ec = 1.6, ε = 1, Nr = 0.3, Pr = 1.7 and various R.

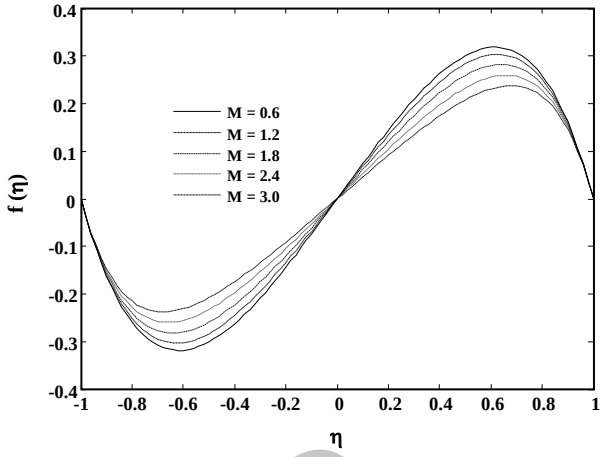

Fig. 9: Variation of axial velocity for R = 5, α = 1, C_1 = 1.4, C_2 = 0.7, C_3 = 1, Ec = 1.6, ε = 1, Nr = 0.2, Pr = 1.7 and various M.

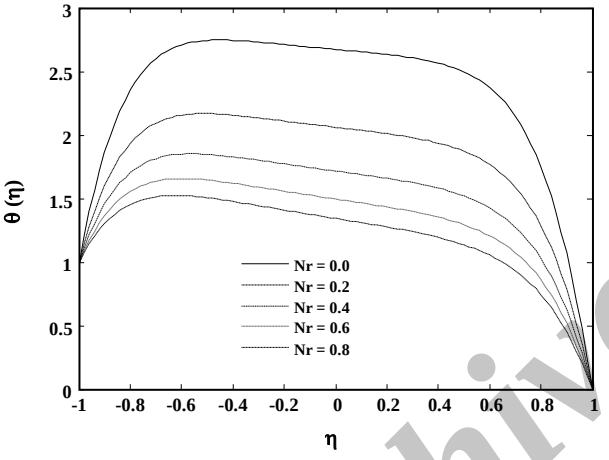

Fig. 7: Variation of temperature for R = 5, α = 1, C_1 = 1, C_2 = 0.2, C_3 = 1, Ec = 1.6, M = 0.5, ε = 1, Pr = 1.7 and various Nr.

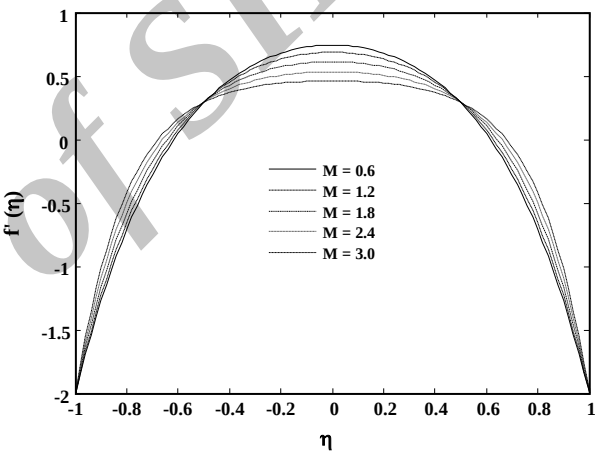

Fig. 10: Variation of radial velocity for R = 5, α = 1, C_1 = 1.4, C_2 = 0.7, C_3 = 1, Ec = 1.6, ε = 1, Nr = 0.2, Pr = 1.7 and various M.

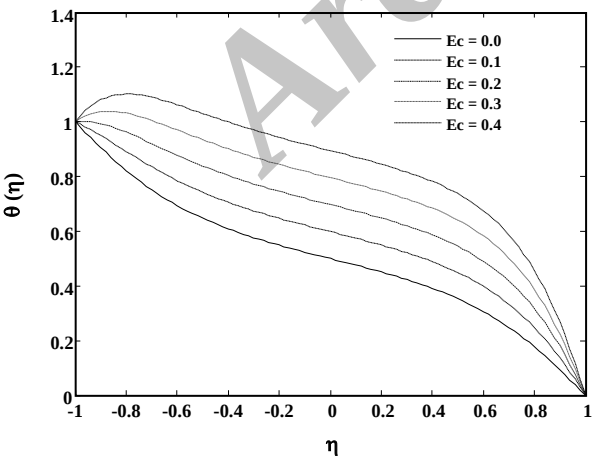

Fig. 8: Variation of temperature for R = 5, α = 1, C_1 = 1.4, C_2 = 0.7, C_3 = 1, Pr = 1.7, M = 0.5, ε = 1, Nr = 0.2 and various Ec.

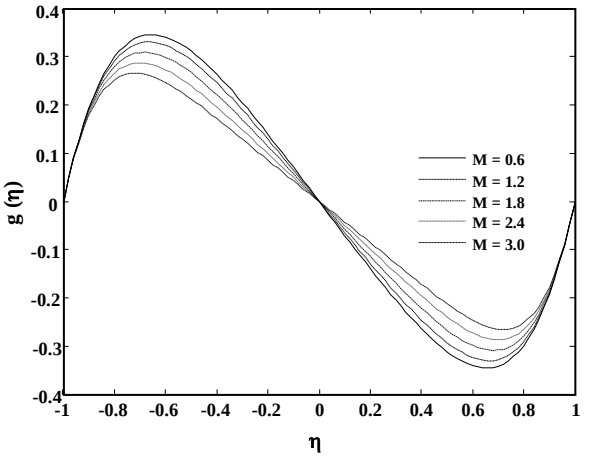

Fig. 11: Variation of microrotation for R = 5, α = 1, C_1 = 1.4, C_2 = 0.7, C_3 = 1, Ec = 1.6, ε = 1, Nr = 0.2, Pr = 1.7 and various M.

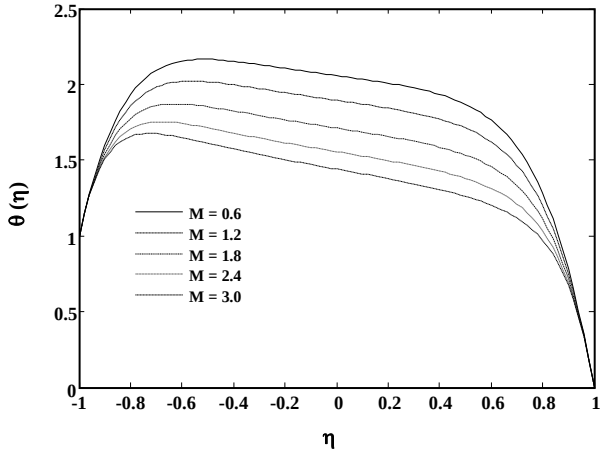

Fig. 12: Variation of temperature for R = 5, α = 1, C_1 = 1.4, C_2 = 0.7, C_3 = 1, Ec = 1.6, ε = 1, Nr = 0.2, Pr = 1.7 and various M.

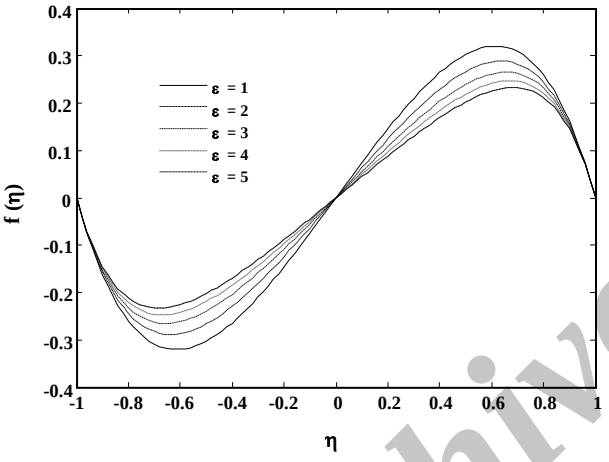

Fig. 13: Variation of temperature for R = 5, α = 1, C_1 = 1.4, C_2 = 0.7, C_3 = 1, Ec = 1.6, M = 1.5, Nr = 0.2, Pr = 1.7 and various ε.

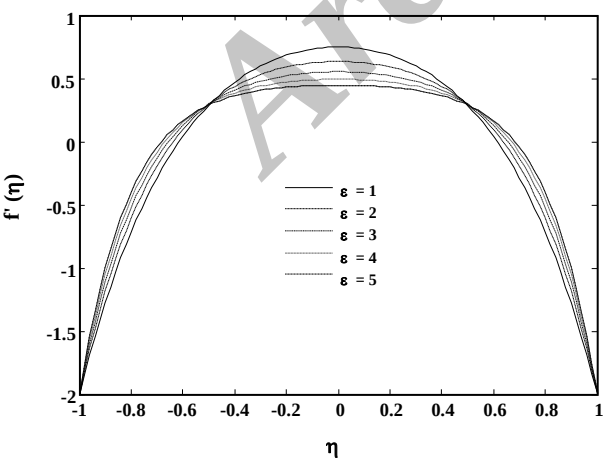

Fig. 14: Variation of temperature for R = 5, α = 1, C_1 = 1.4, C_2 = 0.7, C_3 = 1, Ec = 1.6, M = 1.5, Nr = 0.2, Pr = 1.7 and various ε.

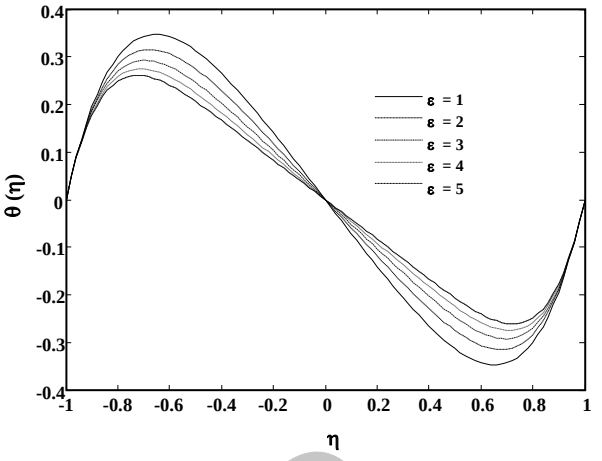

Fig. 15: Variation of microrotation for R = 5, α = 1, C_1 = 1.4, C_2 = 0.7, C_3 = 1, Ec = 1.6, M = 1.5, Nr = 0.2, Pr = 1.7 and various ε.

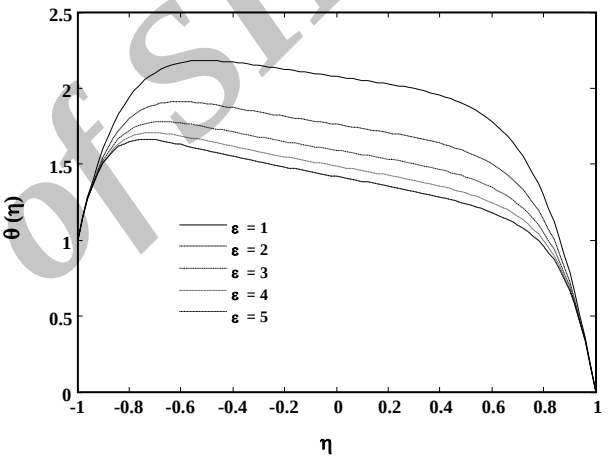

Fig. 16: Variation of temperature for R = 5, α = 1, C_1 = 1.4, C_2 = 0.7, C_3 = 1, Ec = 1.6, M = 1.5, Nr = 0.2, Pr = 1.7 and various ε.

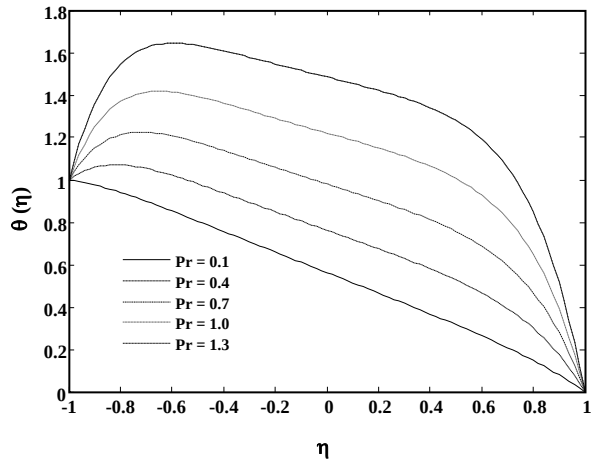

Fig. 17: Variation of temperature for R = 5, α = 1, C_1 = 1.4, C_2 = 0.7, C_3 = 1, Ec = 0, M=0.5, ε = 1, Nr = 0.2 and various Pr.

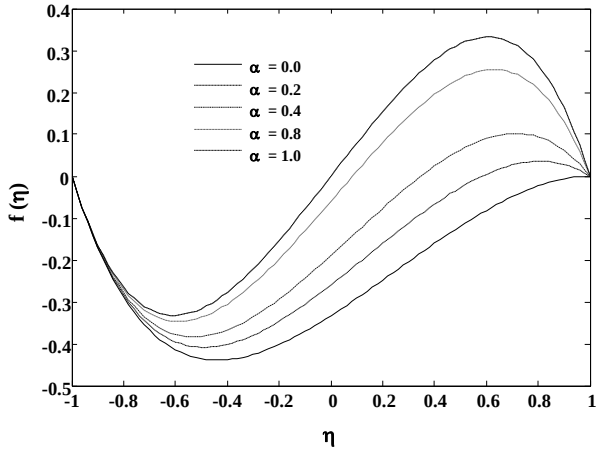

Fig. 18: Variation of axial velocity for R = 4, Ec = 1.6, C_1 = 1.4, C_2 = 0.7, C_3 = 1, Pr = 1.7, M = 0.5, ε = 1, Nr = 0.3 and various α.

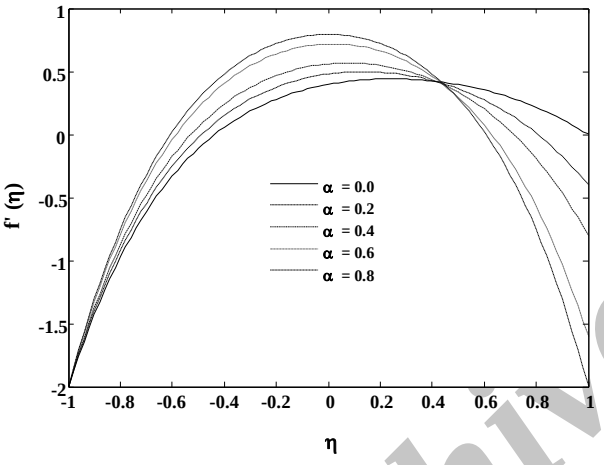

Fig. 19: Variation of radial velocity for R = 4, Ec = 1.6, C_1 = 1.4, C_2 = 0.7, C_3 = 1, Pr = 1.7, M = 0.5, ε = 1, Nr = 0.3 and various α.

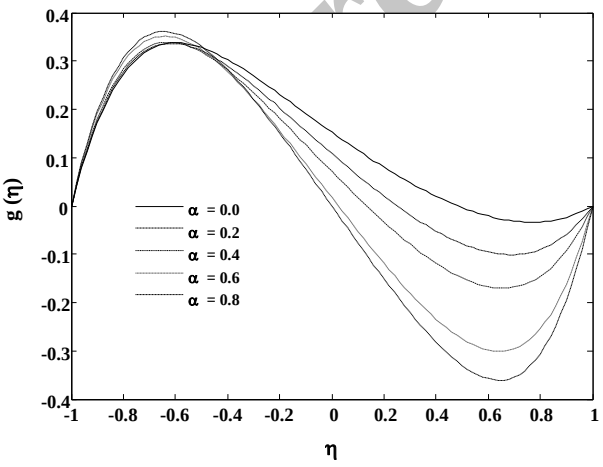

Fig. 20: Variation of microrotation for R = 4, Ec = 1.6, C_1 = 1.4, C_2 = 0.7, C_3 = 1, Pr = 1.7, M = 0.5, ε = 1, Nr = 0.3 and various α.

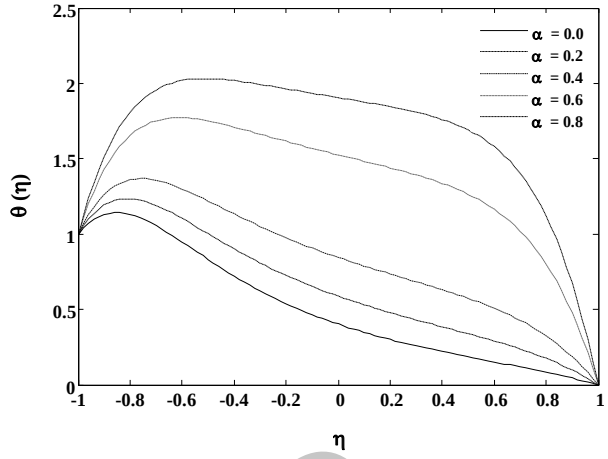

Fig. 21: Variation of temperature for R = 4, Ec = 1.6, C_1 = 1.4, C_2 = 0.7, C_3 = 1, Pr = 1.7, M = 0.5, ε = 1, Nr = 0.3 and various α.

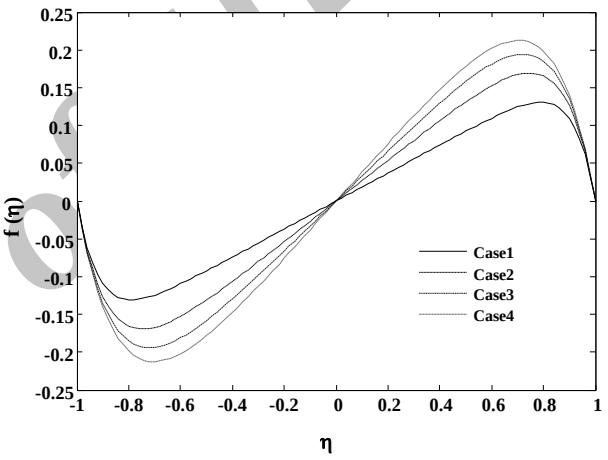

Fig. 22: Variation of axial velocity for R = 5, M = 5, α = 1, Ec = 1.6, ε = 1, Nr = 0.3, Pr = 1.7 and four cases of micropolar parameters.

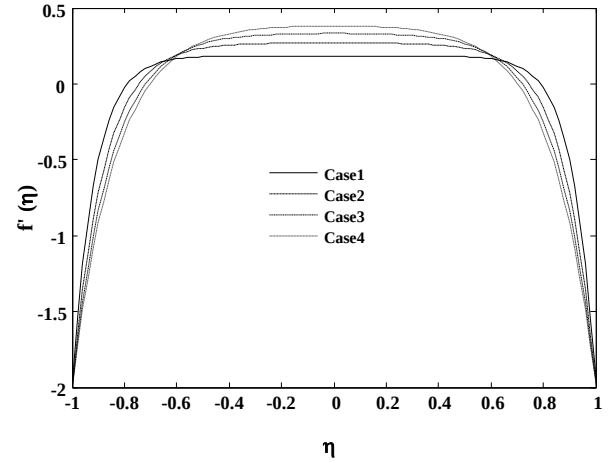

Fig. 23: Variation of radial velocity for R = 5, M = 5, α = 1, Ec = 1.6, ε = 1, Nr = 0.3, Pr = 1.7 and four cases of micropolar parameters.

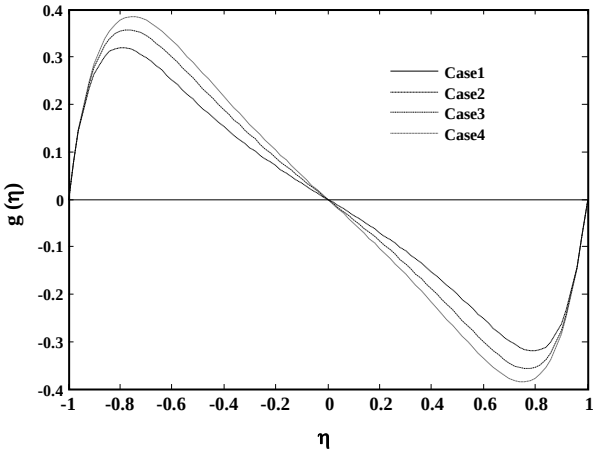

Fig. 24: Variation of microrotation for R = 5, M = 5, α = 1, Ec = 1.6, ε = 1, Nr = 0.3, Pr = 1.7 and four cases of micropolar parameters.

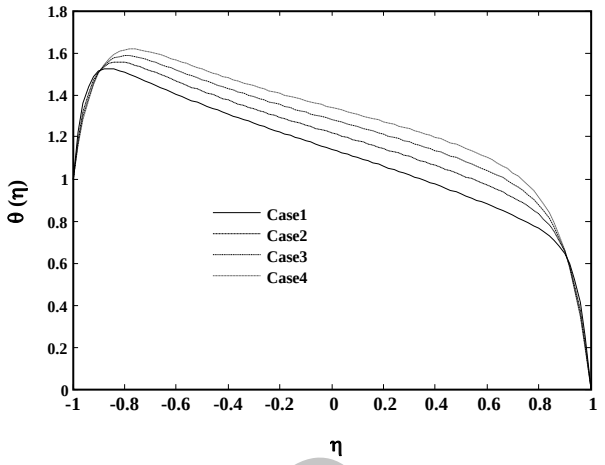

Fig. 25: Variation of temperature for R = 5, M = 5, α = 1, Ec = 1.6, ε = 1, Nr = 0.3, Pr = 1.7 and four cases of micropolar parameters.

CONCLUSIONS

A numerical study is presented for the better understanding of the problem of hydromagnetic flow and heat transfer of micropolar fluid through a porous medium between two stretchable coaxial disks, taking into account the effects of disk stretching, viscous dissipation and thermal radiation.The self-similar nonlinear ODEs, obtained from the governing Navier-Stokes equations, are solved numerically by using an algorithm based on Quasi-linearization and finite discretization. It has been noted that the micropolar structure of the fluid reduces the drag force and the heat transfer rate whereas the stretching of the disks shows the reverse trend. The porosity of the medium has the effect of increasing the shear and couple stresses as well as the heat transfer rate. Finally, the viscous dissipation may cause the thermal reversal near the lower disk.

Nomenclature

u_r , u_z and u_θ	Velocity components along the radial, transverse and axial directions, respectively, m/s
$\upsilon_1, \upsilon_2, \upsilon_3$	The components of microrotation along the radial, transverse and axial directions, respectively kg.m^2
T	Temperature, K
P	Pressure, N/m^2
ρ	Density, kg/m^3
η= (z/h)	Dimensionless similarity variable
$k^\bullet$	Darcy permeability, m^2
μ	Dynamic viscosity, N.s/m^2
B_o	Strength of magnetic field, kg/s^2·A
σ_e	Electrical conductivity, S/m
c_p	Specific heat capacity, J/(kg.K)
q_r	Radiative heat flux, W/m^2
k_o	Thermal conductivity of the fluid, W/(m. K)
σ	Stefan-Boltzmann constant, W/m^{2}K^4
K^*	Mean absorption coefficient
E_1 & E_2	Stretching strengths of the lower and upper disks respectively, 1/s
$M\left(=\sqrt{\frac{\sigma_e B_\circ^{\,2}}{\rho E_1}}\right)$	Magnetic parameter
$C_1=(\kappa/\mu)$	Vortex viscosity
$C_2=\left(j/h^2\right)$	Microinertia density parameter
$C_3=\left(\gamma/\mu h^2\right)$	Spin gradient viscosity parameter
$R=\left(\rho E_1 h^2/\mu\right)$	Stretching Reynolds number
$Ec=\left(r^2 E_1^{\,2}/c_p\left(T_1-T_2\right)\right)$	Eckert number
$Pr=\left(\mu c_p/k_\circ\right)$	Prandtl number
$Nr=\left(4\sigma T_\infty^3/k^* k_\circ\right)$	Radiation parameter
$\varepsilon=\left(h^2/k^\bullet\right)$	Porosity parameter
$\alpha=\left(E_2/E_1\right)$	Relative disk stretching parameter

Acknowledgement

The authors are extremely grateful to the learned reviewers for their comments to improve the quality of the manuscript.

Received : Apr. 15, 2016 ; Accepted : Dec. 26, 2016

REFERENCES

[1] Connor J.J., Boyd J., Avallone E.A., "Standard Handbook of Lubrication Engineering", MC Graw-Hill, New York, USA, (1968).

[2] Darcy H., Les "Fontaines Publiques de la Ville De Pijon", Dalmont, Paris, (1856).

[3] Rashidi M.M., Bour S.A.M., Hayat T., Obadiat S., Analytical Approximate Solutions for Steady Flow Over a Rotating Disk in a Porous Medium with Heat Transfer by Homotopy Analysis Method, *Computers and Fluids*, **54**:1-9 (2012).

[4] Yoon M.S., Hyun J.M., Park J.S., Flow and Heat Transfer Over a Rotating Disk with Surface Roughness, *Int. J. of Heat Fluid Flow*, **28**(2): 262-276 (2007).

[5] Fang T., Tao H., Unsteady Viscous Flow Over a Rotating Stretchable Disk with Deceleration, *Commun. Nonlinear Sci. Numer. Simulation*, **17**:5064-5072 (2012).

[6] Gauthier G., Gondret P., Moisy F., Rabaud M., Instabilities in the Flow Between Co- and Counter Rotating Disks, *J. Fluid Mech.*, **473**:1-21 (2002).

[7] Pesch H.J., Rentrop P., Numerical Solution Of Flow Between Two Counter Rotating Infinite Plane Disks by Multiple Shooting, *ZAMM*, **58**:23-28 (1978).

[8] Hamza M.M., Isah B.Y., Usman H., Unsteady Heat Transfer to MHD Oscillatory Flow Through a Porous Medium Under Slip Condition, *Int. J. Computer Applications*, **33**(4):0975-8887 (2011).

[9] Ali K., Iqbal M.F., Akbar Z., Ashraf M., Numerical Simulation of Unsteady Water- Based Nano Fluid Flow and Heat Transfer Between two Orthogonally Moving Porous Coaxial Disks, *J. Theo. Appl. Mech.*, **52**(4):1033-1046 (2014).

[10] Hoyt J.W., Fabula A.G., "The Effect of Additives on Fluid Friction", *U.S. Naval Ordinance Test Station Report*, (1964).

[11] Eringen A.C., Theory of Micropolar Continua In. "Proceedings of the Ninth Midwestern Conference", (1965).

[12] Eringen A.C., Simple Microfluids, *Int. J. Eng. Sci.*, **2**: 205-217 (1964).

[13] Ashraf M., Wehagal A.R., MHD Flow and Heat Transfer of Micropolar Fluid Between two Porous Disks, *Appl. Math. Mech. Eng. Ed.*,**33**(1):51-60 **(**2012).

[14] Hayat T., Shafiq A., Alsaedi A., Effect of Joule Heating and Thermal Radiation in Flow of Third Grade Fluid over Radiative Surfaces, *Plos One*, **9**(1):e83153 (2014).

[15] Rao A.R., An Exact Solution for Unsteady Flow of a Micropolar Fluid Due to Eccentrically Rotating Disks, *J. Indian Inst. Sci.*, **69**:367-372 (1989).

[16] Ashraf M., Kamal M.A., Syed K.S., Numerical Simulation of a Micropolar Fluid Between a Porous Disk and a Non Porous Disk, *J. Appl. Math. Model.*, **33**:1933-1934 (2009).

[17] Muthu P., Kumar B.V.R., Chandra P., A Study of Micropolar Fluid in an Annular Tube with Application to Blood Flow, *J. Mech. Medi. Bio.*,**8**(4):561-576 (2008).

[18] Ram P., Sharma K., Revolving Ferrofluid Flow Due to Rotating Disk, *Proceedings of The World Congress On Engineering*, **III**: 1913-1917 (2012).

[19] Turkyilmazoglu M., Flow and Heat Simultaneously Induced by two Stretchable Rotating Disks, *J. Physics of Fluids*, **28**: 043601 (2016).

[20] Cai. J., Hua. X., Xiao. B., Zhou. Y., Wei. W., Recent Developments on Fractal-Based Approaches to Nanofluids and Nanoparticle Aggregation, *International Journal of Heat and Mass Transfer*, **105**: 623-637 (2017).

[21] Ashraf M., Kamal M.A., Syed K.S., Numerical Investigations of Asymmetric Flow of a Micropolar Fluid Between two Porous Disks, *Acta Mechanica Sinica*, **25**: 787-794 (2009).

[22] Ashraf M., Kamal MA., Syed KS., Numerical Study of Asymmetric Laminar Flow of Micropolar Fluids in a Porous Channel, *Computer and Fluids*, **38**:1895-1902 (2009).

[23] Ashraf M., Batool K., MHD Flow and Heat Transfer of a Micropolar Fluid Over a Stretching Disk, *J. Theo. Appl. Mech.*, **51**(1):25-38 **(**2013).

[24] Ali K., Ashraf M., Jameel N., Numerical Simulation of Magnetohydrodynamic Micropolar Fluid Flow and Heat Transfer in a Channel with Shrinking Walls, *Canadian Journal of Physics*, **92**: 987-996 (2014).

[25] Ariman T., Turk MA., Sylvester ND., Microcontinuum Fluid Mechanics—A Review, *Int. J. Engineering Sci.*, **11**(8): 905-930 (1973).

[26] Ariman T., Turk M.A., Sylvester N.D., Applications of Microcontinuum Fluid Mechanics, *Int. J. Engineering Sci.*, **12**(4): 273-293 (1974).

[27] Erigen A.C., "Microcontinuum Field Theories", Springer, New York (2001).

[28] Lukaszewicz G., "Micropolar Fields Theory and Applications, Birkhauser", Berlin (1999).

[29] Abolbashari M.H., Freidoonimehr N., Nazari F., Rashidi M.M., Entropy Analysis for an Unsteady MHD Flow Past a Stretching Permeable Surface in Nano-Fluid, *J. Powder Technology*, **267**: 256–267 (2014).

[30] Rashidi M.M., Erfani E., Analytical Method for Solving Steady MHD Convective and Slip Flow Due to a Rotating Disk with Viscous Dissipation and Ohmic Heating, *J. Engineering Computations*, **29**(6): 562-579 (2012).

[31] Rashidi M.M., Ali M., Freidoonimehr N., Rostami B., Hossain M.A., Mixed Convective Heat Transfer for MHD Viscoelastic Fluid Flow over a Porous Wedge with Thermal Radiation, *Advances in Mech. Engineering*, **735939**: (2014).

[32] Rashidi M.M., Momoniat E., Rostami B., Analytical Approximation Solution for MHD Boundary Layer Viscoelastic Fluid Flow Over Continuously Moving Stretching Surface by Homotopy Analysis Method with two Auxialiary Parameters, *J. Applied Mathematics*, (2012).

[33] Aghajani M., Steinhagen H.M., Jamialahmadi M., Heat Transfer of Liquid/ Solid Fluidized Beds for Newtonian and Non-Newtonian Fluids, *Iranian Journal of Chemistry and Chemical Engineering (IJCCE)*, **23**: 119-130 (2004).

[34] Mehrabani M.A., Kimiaeifar AL, Golkarfard V., Akhgar A.R., Study of Chemically Reactive Flow and Heat Transfer in the Presence of a Uniform Magnetic Field, *Iranian Journal of Chemistry and Chemical Engineering (IJCCE)*, **35**: 119-137 (2016).

[35] Akram S., Nadeem S., Hussain A., Influence of Induced Magnetic Field and Partial Slip on the Peristaltic Flow of a Couple Stress Fluid in an Asymmetric Channel, *Iranian Journal of Chemistry and Chemical Engineering (IJCCE)*, **33**(3): 43-52 (2014)

[36] Khan Y., Abdou M.A., Faraz N., Yildirim A., Wu Q., Numerical Solution of MHD Flow Over a Nonlinear Porous Stretching Sheet, *Iranian Journal of Chemistry and Chemical Engineering (IJCCE)*, **31**: 125-132 (2012).

[37] Nadeem S., Akram S., Akbar NS., Simulation of Heat and Chemical Reactions on Peristaltic Flow of a Williamson Fluid in an Inclined Asymmetric Channel, *Iranian Journal of Chemistry and Chemical Engineering (IJCCE)*, **32**: 93-107 (2013)

[38] Shercliff JA., "A Text Book of Magnetohydrodynamics", *Pergamon Press Oxford*, (1965).

[39] Devi S.P.A., Devi R.U., On Hydromagnetic Flow Due to a Rotating Disk with Radiation Effects, *Nonlinear Analysis: Mod. Cont.*, **16**(1):17-29 (2011).

[40] Turkyilmazoglu M., Flow of a Micropolar Fluid Due to a Porous Stretching Sheet and Heat Transfer, *Int. J. of Nonlinear Mechanics*, **83**: 59–64 (2016).

[41] Turkyilmazoglu M., A note on Micropolar Fluid Flow and Heat Transfer Over a Porous Shrinking Sheet, *Int. J. Heat and Mass Transfer*, 72: 388–391 (2014).